Appendix

Appendix figures

Appendix Figure S1. Sequence alignment of CHAV G_{th} and VSV G_{th} (Indiana, Orsay strain)

Appendix Figure S2. Final electron density map for R5 segments.

Appendix Figure S3. Interactions between protomers in CHAV G_{th} intermediate crystal structure.

Appendix Figure S4. Negatively stained VSV particles at 20°C at pH 8, pH 6 and 5.5.

Appendix Figure S5. Negatively stained VSV particles at pH 6.6 and 37°C, pH 6.6 and 4°C and pH 6.2 and 4°C.

Appendix Figure S6. Comparison of the fit of VSV G post-fusion protomer and CHAV G_{th} LI in the tomography reconstruction of VSV G spikes at pH 6.6 and 37°C.

Appendix tables

Appendix Table S1. Statistics of fitting the post-fusion trimer crystal structure into tomography reconstructions of spikes at the surface of VSV incubated at pH5.5 for different threshold values.

Appendix Table S2. Statistics of fitting the post-fusion trimer crystal structure into tomography reconstructions of spikes at the surface of VSV incubated at pH5.5 for different magnification correcting factors.

Appendix Table S3. Statistics of fitting the post-fusion trimer crystal structure into tomography reconstructions of spikes at the surface of VSV incubated at pH5.5.

Appendix Table S4. Statistics of fitting the CHAV G_{th} LI and EI and VSV G_{th} POST conformation crystal structure into tomography reconstructions of spikes at the surface of virions incubated at pH6.6 and 4°C.

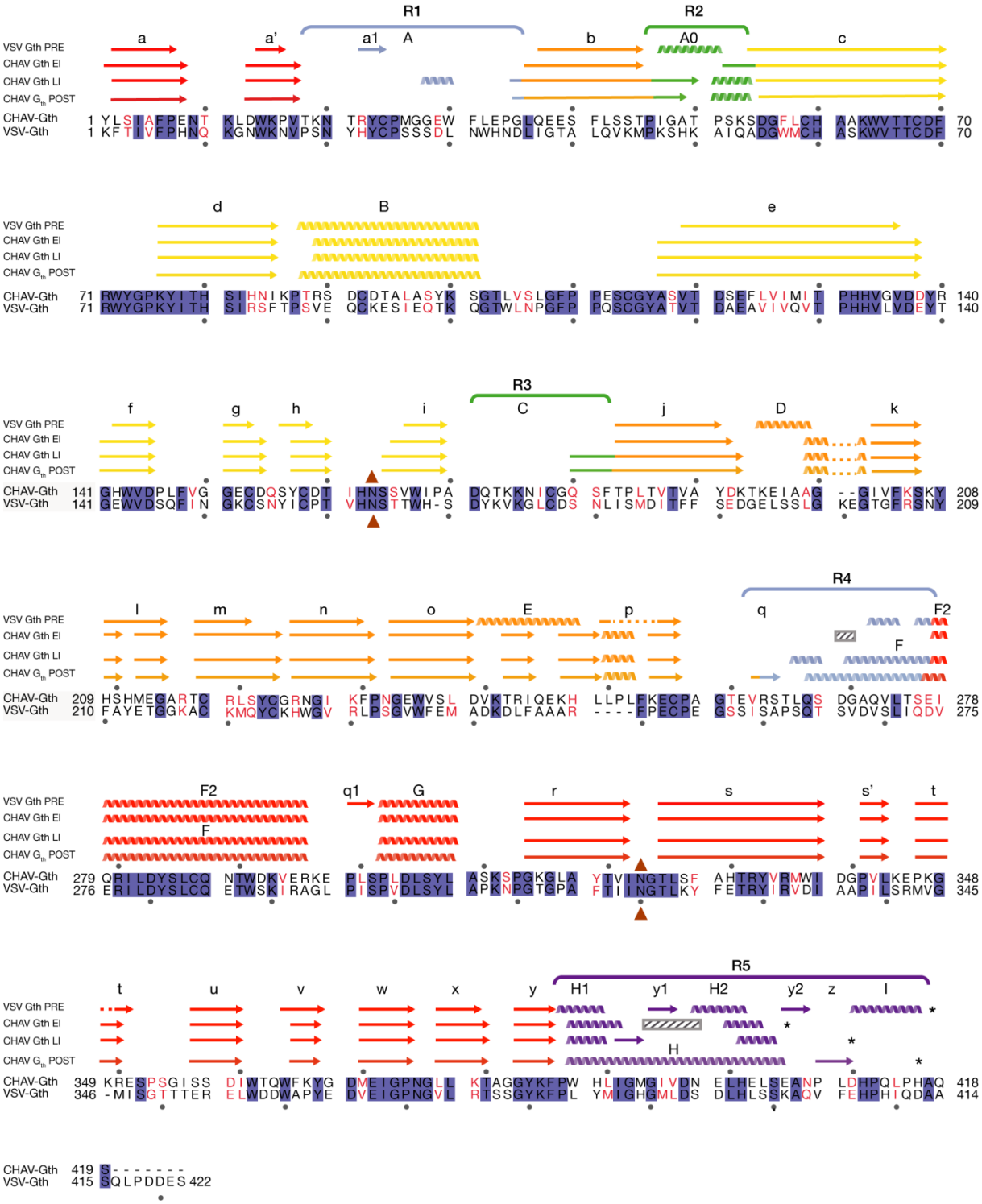

Appendix Figure S1. Sequence alignment of CHAV G_{th} and VSV G_{th} (Indiana, Orsay strain) Conserved residues are in blue boxes whereas similar ones are in red. The black dashes show gaps. Overall aa sequence conservation is 41 %. Elements of secondary structure are indicated above the sequence for the four structures. They are colored as the domain they belong to, with the color code of Table 1. VSV G helices and sheets are named as in Roche et al. (2007). Segments R1 to R5 that refold during the transition are also indicated with the color code of Table 1. Triangles indicate the glycosylation sites. The asterisks indicate the last residue of the molecule for which electron density was still interpretable. Dashed rectangles indicate the parts of the structure where the density was not traceable. A Black dot marks every 10 residues for both CHAV G_{th} and VSV G_{th}.

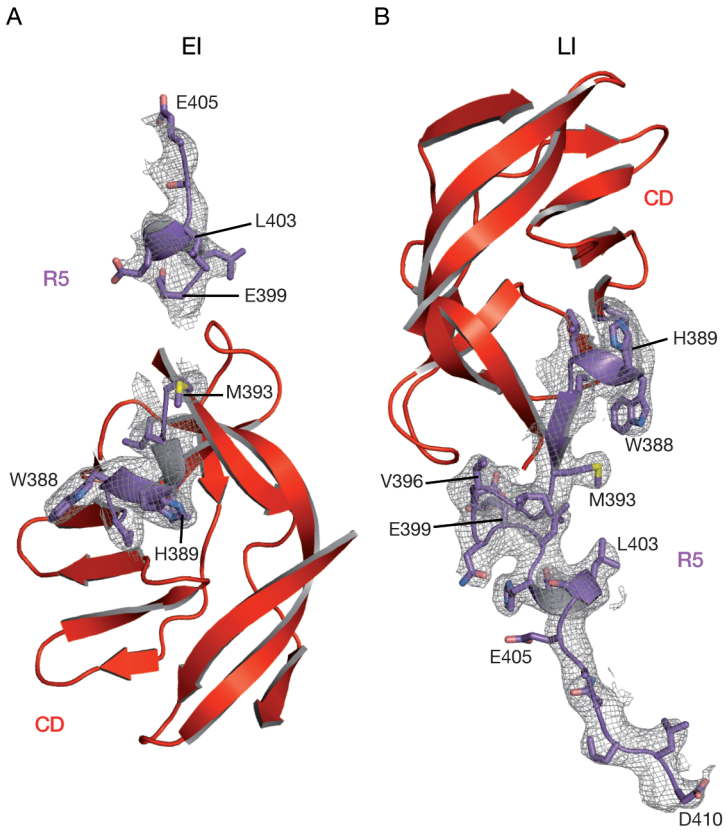

Appendix Figure S2. Final electron density map for R5 segments.
The final 2Fo-Fc electron density map at 3 Å resolution is displayed at 1 sigma contour level as a grey mesh around segment R5 in one EI (**A**) and in one LI (**B**). Segments are displayed in stick representation with nitrogens in blue, oxygens in red, sulphurs in yellow and carbons colored by domains with standard colors (as defined in Table 1).

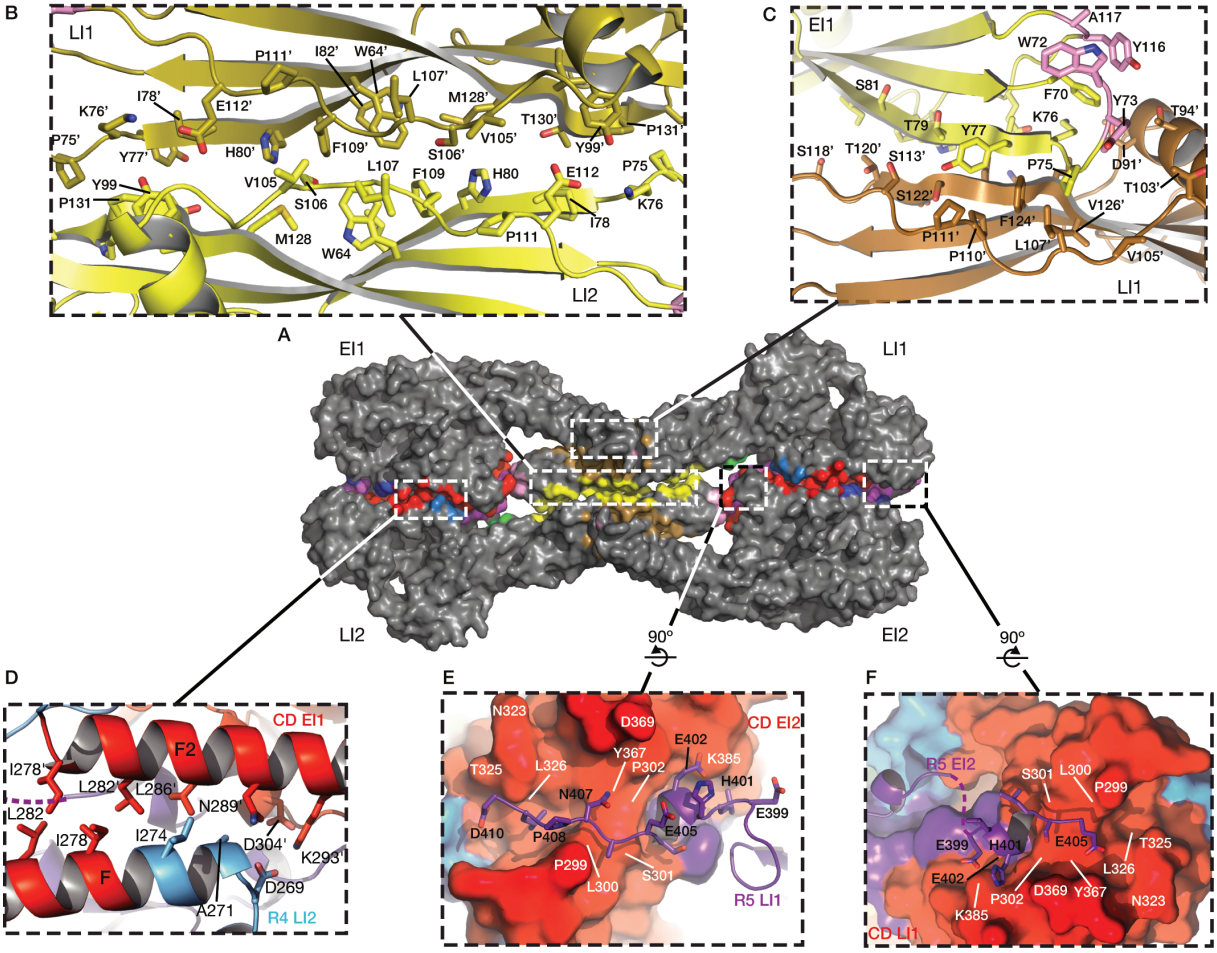

Appendix Figure S3. Interactions between protomers in CHAV Gth intermediate crystal structure.

(A) Overall view of the buried interfaces in the crystalline dimer of heterodimers. The interfaces are colored as indicated in Table 1 according to the domains and segments they belong to, except the FD interfaces buried between EI and LI which are in brown. Dashed boxes indicate the interface regions which are presented below as close-up views.

(B) Close up view of the interaction between LI1 and LI2 FDs. Interface residues are displayed as sticks. They are labeled for one LI molecule and labeled with ' for the other.

(C) Close up view of the interaction between EI1 (in yellow) and LI1 (in brown) fusion domains. Hydrophobic residues from EI1 and LI1 which cluster below the exposed EI2 fusion loops (in pink) are represented in sticks and labeled, with ’ for LI1 residues. Note the extended hydrophobic surface next to the EI fusion loops which is largely located on LI.

(D) Close up view of the F2/F antiparallel interaction area in a CHAV Gth EI1 / LI2 CD interaction. EI1 residues are labeled with ’

(E,F) Close up views of the interactions between R5 segments (drawn as a ribbon) and the hydrophobic groove of the CDs (in surface view). Residues of the R5 segment involved in the interaction are in sticks and indicated with black labels. Residues on the CD involved in the interaction are indicated with white labels. (E) The C-terminal part of the LI1 R5 segment is located within the CD groove of EI2. (F) The C-terminal part of the EI2 R5 segment is located within the CD groove of LI1.

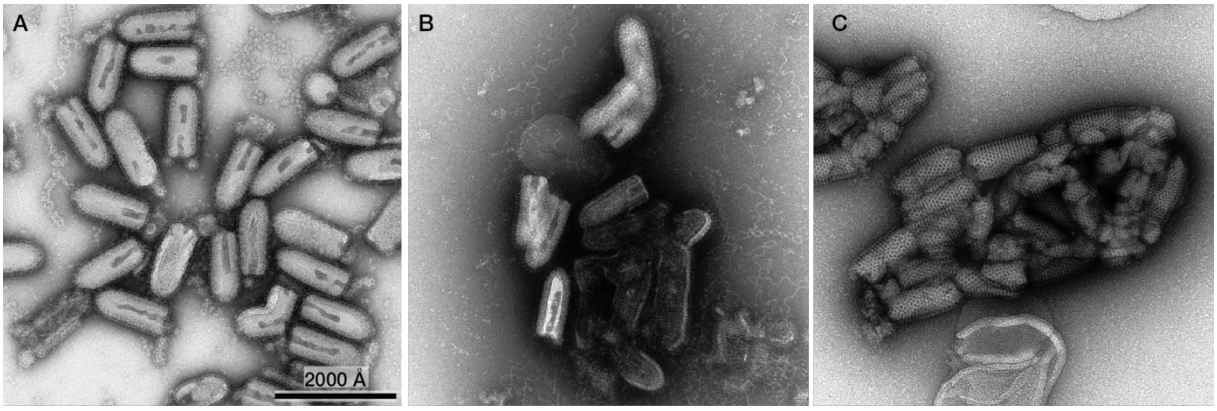

Appendix Figure S4. Negatively stained VSV particles at 20°C and pH 8 (A), pH 6 (B) and 5.5 (C).

All images are at the same magnification (scale bar in A).

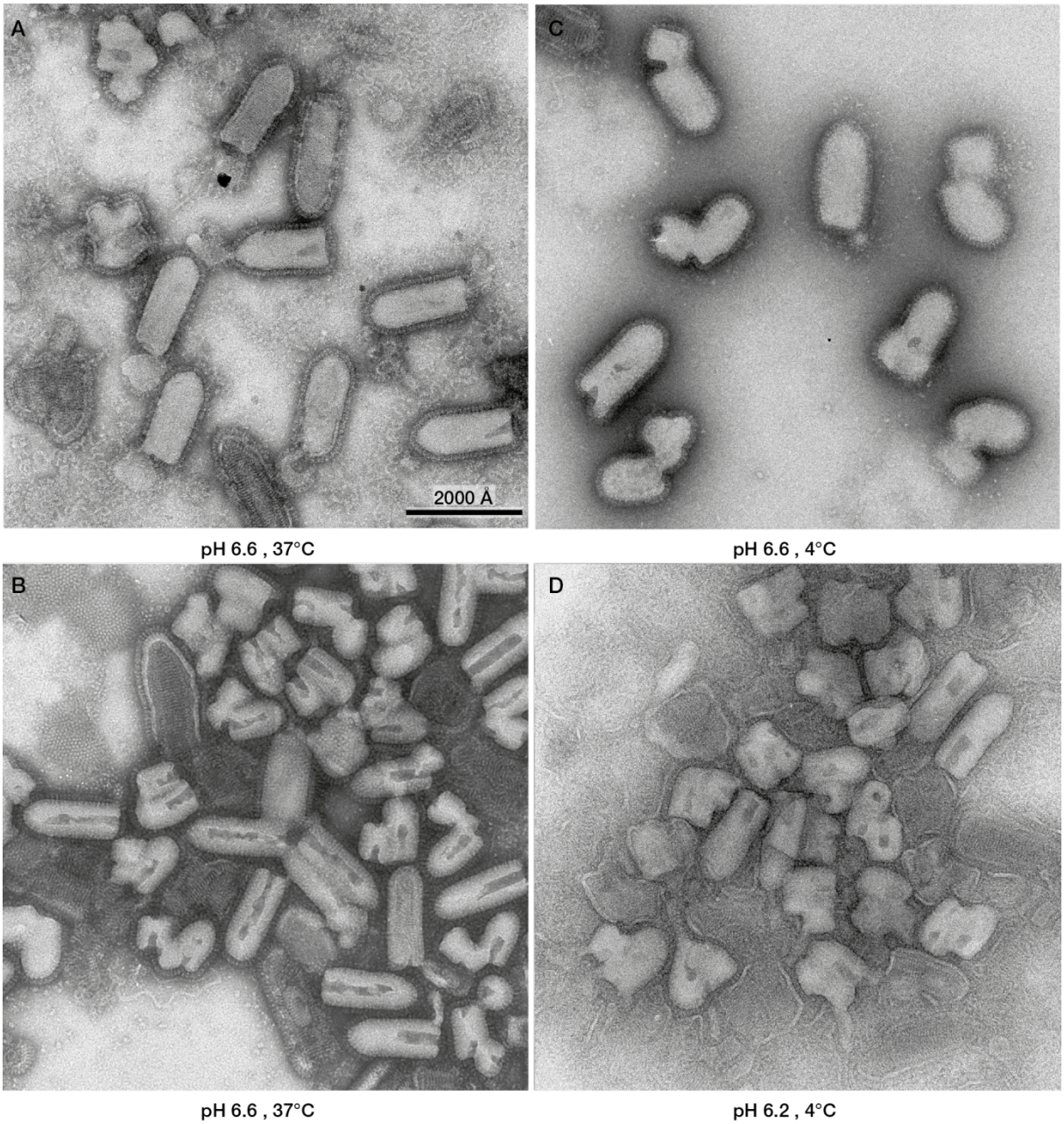

Appendix Figure S5. Negatively stained VSV particles at pH 6.6 and 37°C (A, B), pH 6.6 and 4°C (C) and pH 6.2 and 4°C (D).

At pH 6.6 and 37°C, aggregation and fusion of viral particles are dependent on viral concentration (the concentration of viral particles is higher in B than in A). At pH 6.6 and 4°C (C), thin and elongated spikes are observed at the viral surface (see also Figure 5H and 5L) but no aggregation is detected, which suggests that the fusion loops are not exposed but rather pointing toward the viral membrane. At pH 6.2 and 4°C, both aggregation and fusion between viral particles are observed. All images are at the same magnification (scale bar in A).

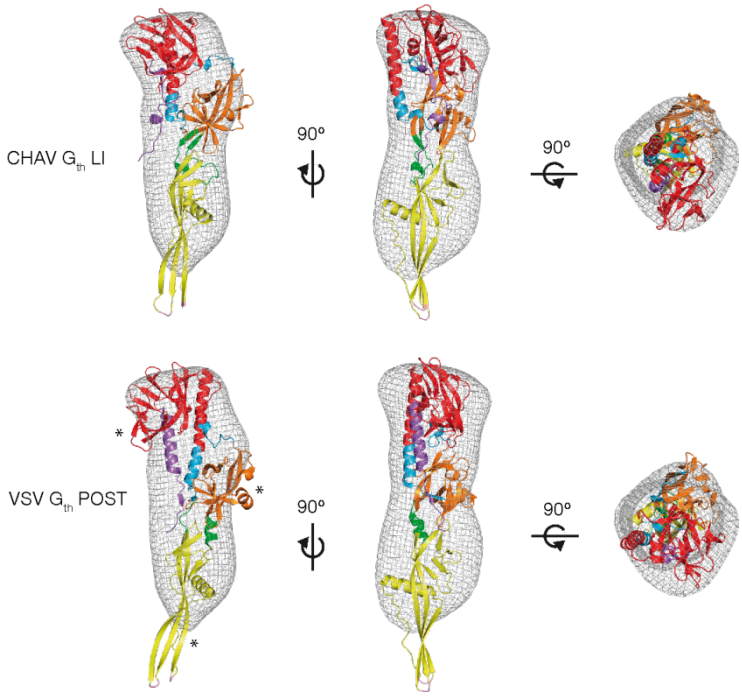

Appendix Figure S6.
Comparison of the fit of VSV G post-fusion protomer and CHAV G_{th} LI in the tomography reconstruction of VSV G spikes obtained after negative staining in hydration-preserving conditions at pH 6.6 and 37°C. Consistent with the statistics data presented, in table S5, the best fit is obtained with CHAV G_{th} LI. Asterisks indicate the regions of G which degrade the R factor of the post-fusion state fit.

Threshold value	R factor values (%)
0.0	44.3; 24.8
0.25	44.1; 23.2
0.5	41.6; 21.2
0.75	40.2; 18.8
1.0	**37.9; 18.7**
1.25	38.9; 20.0
1.5	39.3; 21.4
2.0	41.5; 29.9

Appendix Table S1. Statistics of fitting the post-fusion trimer crystal structure into tomography reconstructions of spikes at the surface of VSV incubated at pH5.5 for different threshold values.
R-factor values calculated with the non-symmetrized experimental map and the fitted post-fusion crystallographic trimer model for different threshold values. The R factor values have been calculated for the 150-35 (first value) and the 150-45 Å (second value) resolution ranges. In bold are indicated the lowest values of the R factor and thus the optimized threshold value: 1.0.

Magnification correcting factor	R factor values (%) Non-symmetrized map	R factor values (%) Symmetrized map
1.02	36.8; 19.3	36.1; 15.3
1.01	38.0; 18.5	36.6; 14.8
1.00	37.9; 18.7	36.5; 13.6
0.99	37.2; **18.4**	36.7; **12.9**
0.98	**35.9**; 18.6	34.9; 13.2
0.97	36.1; 19.1	**34.4;** 13.9
0.96	36.3; 19.5	34.6; 14.9

Appendix Table S2. Statistics of fitting the post-fusion trimer crystal structure into tomography reconstructions of spikes at the surface of VSV incubated at pH5.5 for different magnification correcting factors.
R-factor values calculated with the non-symmetrized and the C3 symmetrized experimental maps and the fitted crystallographic post-fusion trimer model for different magnification correcting factors. The R factor values have been calculated for the 150-35 (first value) and the 150-45 Å (second value) resolution ranges. In bold values indicated the lowest R factor and thus the optimized magnification correcting value: 0.99

Fitting resolution range (Å)	R factor values (%)
150-30	45.9 (**42.6**; 48.4)
150-35	**36.7** (39.0; 38.1)
150-40	**22.2** (27.8: 23.1)
150-45	**12.9** (19.2; 16.6)
150-50	**13.9** (18.5; 15.5)

Appendix Table S3. Statistics of fitting the post-fusion trimer crystal structure into tomography reconstructions of spikes at the surface of VSV incubated at pH5.5.
R-factor values calculated with the symmetrized experimental map and the fitted model constituted by the crystallographic post-fusion trimer. In brackets are the values calculated with the non-symmetrized EM map or with an inverted map.

Fitting resolution range (Å)	R factor values (%) LI monomer	R factor values (%) POST monomer	R factor values (%) EI monomer
150-30	48.8 (47.6)	57.3	56.1
150-35	35.1 (35.8)	43.6	44.2
150-40	32.4 (33.8)	38.7	41.6
150-45	23.2 (25.9)	26.1	29.9
150-50	22.6 (22.7)	25.2	25.8

Appendix Table S4. Statistics of fitting the CHAV G_{th} LI and EI and VSV G_{th} POST conformation crystal structure into tomography reconstructions of spikes at the surface of virions incubated at pH6.6 and 4°C.
R-factor values are calculated with the experimental map and the fitted model (CHAV LI, EI and VSV POST monomer) for different resolution ranges. In brackets are the values calculated with an inverted map.